Cite this article
Neeraj CR and Thiyyakkandi S (2021)
Factor of safety of pile-stabilised slopes: an algorithm incorporating soil-arching effect.
Geotechnical Research **8(4)**: 117–129,
https://doi.org/10.1680/jgere.21.00013

Research Article
Paper 2100013
Received 09/06/2021; Accepted 29/07/2021
Published online 19/10/2021

Geotechnical Research

ice Publishing

Factor of safety of pile-stabilised slopes: an algorithm incorporating soil-arching effect

C. R. Neeraj MS
PhD Research Scholar, Department of Civil Engineering, Indian Institute of Technology Palakkad, Kerala, India (Orcid:0000-0001-9837-0496)

S. Thiyyakkandi PhD
Assistant Professor, Department of Civil Engineering, Indian Institute of Technology Palakkad, Kerala, India (Orcid:0000-0002-5857-9970)
(corresponding author: sudheesh@iitpkd.ac.in)

The current practice of factor of safety computation of pile-stabilised slopes depends substantially on either the extension of methods for normal slopes with the pile-contribution introduced as an additional term or finite-element modelling. Extending conventional methods to analyse pile-stabilised slopes fails to capture the key mechanisms like soil arching, gradual transfer of resistance offered by the pile through the slope, change in slip surface due to introduction of piles and so on. In this paper, a new algorithm is proposed to compute the factor of safety of pile-stabilised slopes, in which the Morgenstern–Price method is modified to incorporate the effect of a pile. The resistance offered by the pile is obtained using a pressure-based method which considers the soil-arching effect in horizontal and vertical directions. The gradual propagation of this resistance offered by the pile is incorporated through an iterative procedure, unlike the conventional methods. The algorithm considers the change in slip surface due to the introduction of the pile. The factor of safety values computed using the proposed algorithm were found to be in close agreement with that obtained from finite-element modelling. Moreover, a simple technique to determine the optimal location of stabilising piles and pile-spacing is also presented.

Keywords: failure/piles and piling/slope stabilisation/slopes

Notations

D diameter of stabilising piles
E modulus of elasticity
E_i normal inter-slice force
F_s Factor of safety of slope
H depth of the pile above the slip surface
K_{an} new coefficient of lateral earth pressure incorporating soil arching
K_c horizontal seismic coefficient
M_s additional moment due to installation of the piles
N_i' effective normal force on the base
P lateral resistance offered by the pile per unit depth
P_i resultant lateral force acting on post-arching zone
P_o resultant reaction on pre-arching zone
P_r resultant lateral force on pile
Q_i external force on (i^{th}) slice
S_i' mobilized shear resistance on the base of a slice
U resultant pore water force
W_i self-weight of i^{th} slice
X inter-slice shear force
b_i width of i^{th} slice
c cohesion of the soil
h_i height of i^{th} slice
l_a length of horizontal arching zone
n ratio of centre-to-centre spacing and pile diameter
s centre-to-centre spacing between piles
u average pore water pressure
α_i base inclination of i^{th} slice
β angle of soil slope with horizontal
γ unit weight of soil
Λ spacing coefficient
λ scale factor
λ_m proposed scale factor
μ Poisson's ratio
ϕ angle of internal friction of soil
Ψ angle of dilatancy of soil
σ_i radial stress on the inner arch of horizontal arching zone
$\overline{\sigma}_v$ average vertical stress on a differential element dz

Introduction

The stability of slopes is one of the fundamental problems in geotechnical engineering as their delicate balance is often disrupted by natural or man-made causes. Furthermore, the increasing demand for engineered cut-and-fills, construction near or on slopes and so on, has increased the need to understand the mechanism of slope failure and develop techniques to stabilise the slopes. Stability of slopes depends on the balance between a driving force that causes failure and a resisting force that is developed against it. All the slope stabilisation methods basically try to reduce the driving force or increase the resisting force or both. One of the operative techniques employed for stabilisation of slopes and prevention of excessive soil movement is using stabilising piles in row(s) (Ashour and Ardalan, 2012; Ausilio *et al*., 2001; Cai and Ugai, 2000; Hassiotis *et al*., 1997; Ito and Matsui, 1975; Kourkoulis *et al*. 2011a; Liang *et al*. 2014; Lirer, 2012; Neeraj and Thiyyakkandi, 2020). In practice, the piles are installed well beyond the potential slip surface to the firm ground beneath it to arrest the possible sliding of unstable soil mass. The piles act as a cantilever beam that takes the lateral forces due to the sliding soil mass and transfer them to the stable ground underneath it (Ellis *et al*., 2010; Liang and Zeng, 2002). This additional resistance provided by the piles stabilises the slope, thus

improving its factor of safety (F_s) against failure. The computation of F_s of pile-stabilised slopes is conventionally done by extending the methods used for analysis of normal slopes to incorporate the additional forces generated due to installation of piles.

The stability of normal slopes can be analysed by numerous methods such as the limit analysis method, variational calculus method, strength reduction method, limit equilibrium method and so on (Atarigaya, 2016). The need for considering different forces (e.g. body force, pore water pressure, etc.) and diverse soil types in the stability analysis of slopes invalidates the use of conventional methods in the mechanics of continua, and consequently, the limit equilibrium method is commonly adopted (Morgenstern and Price, 1965). One of the earliest known and most widely used concepts of limit equilibrium is explained through method of slices owing to the ease of computation (Ahmed, 2017; Atarigaya, 2016; Duncan, 1996; Firat, 2009; Hassiotis *et al*., 1997; Tsuchida and Athapaththu 2014; Zhu *et al*., 2005). The analysis is done by dividing the slope into a number of slices to find out the factor of safety of the slope. Various methods commonly used for formulation of F_s in the method of slices are the Fellenius Swedish circle or ordinary method, Bishop's simplified method, Janbu method, Spencer method and Morgenstern–Price method. All these limit equilibrium methods use the Mohr–Coulomb criterion to determine the shear strength of soil along the failure surface. The choice of method depends largely on the type of soil and the required accuracy of the work. The most widely used method for the analysis of a generalised slip surface is the Morgenstern–Price method (Ahmed, 2017; Atarigaya, 2016; Firat, 2009; Griffiths and Lane, 1999). This method considers both moment and force equilibriums to produce a non-linear indeterminate equation for F_s. The equation is made determinate by assuming a function that relates the inter-slice shear force to inter-slice normal force.

The methods mentioned above are applicable for the case of normal slopes that are not stabilised by piles. At present, the study of pile-stabilised slopes is generally carried out by extending these conventional methods (Di Laora *et al*., 2017; Firat, 2009; 1995; Jeong *et al*., 2003; Kourkoulis *et al*., 2011; Lee *et al*., 1995, Summersgill *et al*., 2018). The resistance offered by the piles is added as an additional term in the formulation of F_s, which does not account for the propagation of reactive force through soil. A major issue in this approach is that the critical slip surface considered is the same as that of non-stabilised soil slopes (Firat, 2009; Kourkoulis *et al*., 2011; Lee *et al*., 1995; Summersgill *et al*., 2018). However, in reality, due to the introduction of piles, the critical slip surface changes and this modified surface needs to be considered while computing the F_s. Also, the conventional methods fail to incorporate the effect of location of piles along the slopes (Hassiotis *et al*., 1997; Lirer, 2012; Neeraj, 2019; Summersgill *et al*., 2018). In the present study, the Morgenstern–Price method is modified using the method of slices to adopt for the analysis of pile-stabilised slopes such that the cumulative effect of lateral resistance offered by the pile on each slice is accounted for. An algorithm is developed to compute the F_s of the pile-stabilised slope considering the modified critical slip surface. The proposed algorithm can be easily switched to use for both normal slopes and pile stabilised slopes. Finite-element modelling of both normal and pile-stabilised slopes was carried out and the obtained F_s values were used to validate the proposed algorithm. The variation of F_s with the location of the pile along the slope was studied. Subsequently, a simple technique to determine the optimal pile location is explained.

The F_s computation using the proposed algorithm requires accurate determination of lateral resistance offered by the stabilising piles. Due to the resistance from the pile and differential movement of soil in between the piles, the soil-arching effect plays a key role in the load-transfer mechanism of pile-stabilised slopes. Several methods have been proposed in the past to estimate the lateral resistance offered by the row of piles incorporating the effect of soil arching. One of the pioneering attempts to model the soil-arching effect due to the differential lateral deformation of soil between the piles in the horizontal direction (termed as 'squeezing effect') was by Ito and Matsui (1975). However, the method does not consider the rotation of principal stresses due to soil arching. Most of the methods developed afterward have adopted or modified the 'squeezing concept' considered by Ito and Matsui (1975) (Fırat 2009; Harrop-Williams, 1989; He *et al*., 2015a; He *et al*., 2015b; Li and Wei, 2018; Song *et al*., 2012; Won *et al*., 2005). As the soil in front of the piles deforms vertically, the lateral earth pressure distribution adjacent to the stabilising piles will become non-linear due to the vertical arching. Adopting the formulation of Ito and Matsui (1975), He *et al*. (2015a) presented an analytical method to determine the non-linear pile resistance in sandy slopes incorporating vertical arching. The method was extended by He *et al*. (2015b) for c–ϕ soil; however, it does not account for the effect of slope angle. In reality, both horizontal and vertical arching need to be considered to determine the lateral resistance offered by the stabilising piles. Recently, Neeraj and Thiyyakkandi (2020) presented a general method (for c–ϕ soil) to determine the lateral pile resistance incorporating the effect of soil arching in horizontal and vertical directions. The method also considers the effect of slope angle (β) in the design. In this work, the method of Neeraj and Thiyyakkandi (2020) is extended to model the gradual propagation of pile resistance as explained in subsequent sections.

Lateral resistance offered by the row of piles

An analytical method to obtain the lateral resistance offered by the row of piles considering the effect of soil arching in both the horizontal and vertical direction was proposed by Neeraj and Thiyyakkandi (2020). The stress state of the soil-arching zone in the horizontal direction is presented in Figure 1. The resistance offered by the stabilising piles is given by:

$$P = \sigma_i(\Lambda + 1)D + \frac{2c\sqrt{N}}{N-1}\Lambda D \quad (1)$$

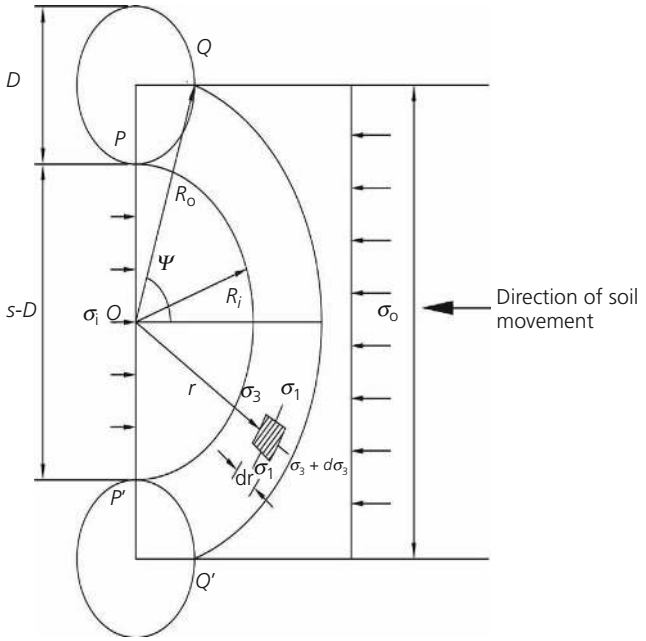

Figure 1. Horizontal arching zone in pile-stabilised slopes

Where, Λ is the spacing coefficient given by, $\Lambda = [(\frac{\sqrt{n^2+1}}{n-1})^{N-1} - 1]n$; here n is the ratio of pile spacing to the diameter of the piles ($n = s/D$) and $N = \tan^2 45 + \phi/2$. The term c represents the cohesion of the soil, and ϕ the angle of internal friction. The stress, σ_i, acting along the central plane of pile row is a function of average vertical stress ($\overline{\sigma}_v$) as given by:

$$\sigma_i = K_{an}\overline{\sigma}_v + T \quad (2)$$

Where:

$K_{an} = \frac{\cos(\theta_w+\xi)\cos\beta}{\cos(\beta+\xi)}\left[\frac{3(N\cos^2\theta_w+\sin^2\theta_w)}{3N-(N-1)\cos^2\theta_w}\right]$

$T = \frac{2c}{\sqrt{N}}\left[\frac{\cos^2\theta_w(3(N\cos^2\theta_w+\sin^2\theta_w))}{3N-(N-1)\cos^2\theta_w} - \sin^2\theta_w\right]$

The stress state including the direction of the major and minor principal stresses after vertical arching in the active plastic zone behind the row of piles is shown in Figure 2. A differential element $EFF'E'$ is assumed to take a circular shape due to vertical arching caused by the shear resistance developed along the vertical plane OB. An intricate analysis considering the force equilibrium of the differential element results in the formulation of an expression for average vertical stress, $\overline{\sigma}_v$, given by (Figure 2):

$$\overline{\sigma}_v = \frac{\gamma\cos\beta H}{1-C_1}\left[\left(1-\frac{z}{H}\right)^{C_1} - \left(1-\frac{z}{H}\right)\right] + \frac{C_2}{C_1}\left[\left(1-\frac{z}{H}\right)^{C_1} - 1\right] \quad (3)$$

Where:

$C_1 = (K_{an}\tan\phi - K_{an}\tan\beta + m)\frac{\sin\theta}{\cos\theta_1}$; $m = \frac{K_{an}}{N\cos^2\theta+\sin^2\theta}\frac{\sin\xi\cos\beta}{\cos(\xi+\beta)}$

$C_2 = (T\tan\phi - K_{an}\tan\beta + t)\frac{\sin\theta}{\cos\theta_1}$;

$t = c + (\frac{T+2c\sin^2\theta/\sqrt{N}}{N\cos^2\theta+\sin^2\theta})\frac{\sin\xi\cos\beta}{\cos(\xi+\beta)}$

where, θ is the angle between the slip plane and the slope surface; θ_1 is the angle between the slip plane and the horizontal; β is the slope angle; and ξ is the angle between the major principal stress and vertical at point where the differential element dz intersects the slip plane; which are given by:

$\xi = \frac{\pi}{4} + \frac{\phi}{2} - \theta_1$; $\theta = \frac{1}{2}(\phi - \beta + \cos^{-1}\frac{\sin\beta}{\sin\phi})$; and $\theta_1 = \frac{1}{2}(\phi + \beta + \cos^{-1}\frac{\sin\beta}{\sin\phi})$

The average vertical stress ($\overline{\sigma}_v$) varies non-linearly with depth of the pile due to the vertical arching of soil. The detailed derivation of Equation 3 is presented in Appendix A.

The resultant force (P_r) offered by the row of piles can be obtained by integrating Equation 1 with respect to the depth of the pile:

$$P_r = D(\Lambda+1)K_{an}\left[\frac{\gamma\cos\beta\ H^2}{1-C_1}\left(\frac{1}{1+C_1}-\frac{1}{2}\right) + \frac{C_2H}{C_1}\left(\frac{1}{1+C_1}-1\right)\right] + TD(\Lambda+1)H + \frac{2c\sqrt{N}\ \Lambda DH}{N-1} \quad (4)$$

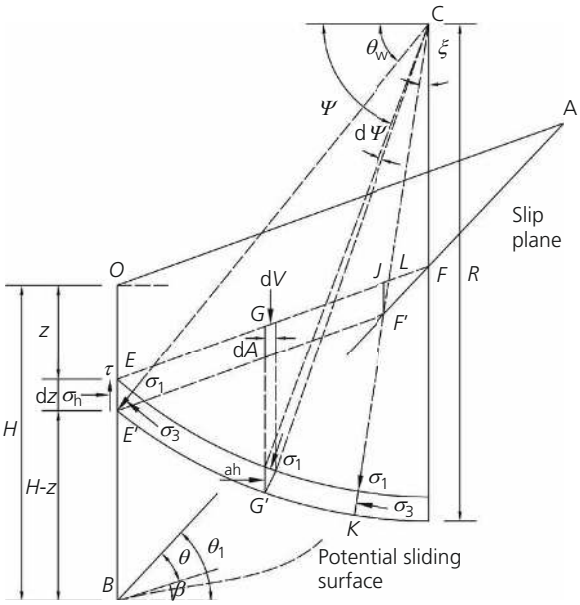

Figure 2. Stress state of vertical arching zone in front of pile row

Further details about the derivations of Equations 1–4 can be found in the paper by Neeraj and Thiyyakkandi (2020). The analytical method described above is adopted to obtain the lateral resistance offered by piles. The method is further extended in this work to be used in the determination of F_S of pile-stabilised slopes as explained in the following section.

Analytical solution for safety analysis

As mentioned in the Introduction, the Morgenstern–Price method is used in this study to analyse slope stability. According to Morgenstern and Price (1965), the inter-slice shear forces (X_i) can be related to inter-slice normal forces (E_i) by a predefined function $f(x)$ as given in Equation 5. The direction of inter-slice forces varies according to the assumed function.

$$X_i = E_i \lambda f(x) \quad (5)$$

Where:

$f(x)$ = inter-slice function that varies continuously along the slip surface

λ = scale factor for the assumed function

Theoretically, the force function $f(x)$ can take any form. However, the nature of soil imposes certain range of functions that can be rationally used for all practical purposes (Morgenstern and Price, 1965). Commonly used functions are constant, half-sine, trapezoidal, user-defined, and so on. In this analysis, $f(x)$ is assumed as a half-sine function. An algorithm, based on the Morgenstern–Price method, developed by Zhu *et al*. (2005) to determine the F_s for soil slopes that are not stabilised by piles is modified to incorporate the effects of additional reactive forces generated due to the introduction of stabilising piles. The solution is developed such that both moment equilibrium and force equilibrium are satisfied.

Figure 3 shows the free-body diagram of a typical slice (i^{th}) with height h_i, width b_i and base inclination α_i. The slice is subjected to a self-weight W_i and seismic force K_cW_i, where K_c is the horizontal seismic coefficient, with external force Q_i acting at an angle ω_i to the vertical, resultant pore water force $U_i = u_i b_i \sec \alpha_i$, where u_i is the average pore water pressure, effective normal force on the base N_i' and mobilized shear resistance $S_i = (N_i' \tan \phi_i' + c_i' b_i \sec \alpha_i)/F_s$, where ϕ_i' is the effective angle of internal friction, c_i' is the cohesion along the base of the slice and F_s is the factor of safety for the slip surface. F_s is assumed to be constant along a slip surface. The soil slice is also subjected to normal inter-slice forces E_i and E_{i-1} on the left and right boundaries of the slice at a height z_i and z_{i-1} from the bottom, respectively. Inter-slice shear forces are calculated using Equation 5.

The equation for F_s developed by Zhu *et al*. (2005) based on the Morgenstern–Price method for soil slopes that are not stabilised by piles is as given below.

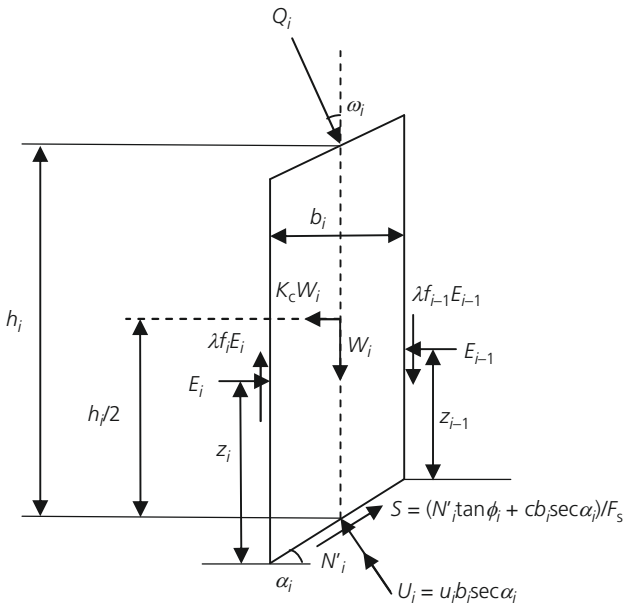

Figure 3. Free body diagram of a typical slice

$$F_s = \frac{\sum_{i=1}^{n-1}\left[R_i \prod_{j=1}^{n-1}\Psi_j\right] + R_n}{\sum_{i=1}^{n-1}\left[T_i \prod_{j=1}^{n-1}\Psi_j\right] + T_n} \quad (6)$$

Where:

$$\Psi_i = \left[(\sin\alpha_i - \lambda f_{i-1}\cos\alpha_i)\tan\phi_i' + (\cos\alpha_i + \lambda f_{i-1}\sin\alpha)F_s\right]\Phi_{i-1} \quad (7)$$

$$\lambda = \frac{\sum_{i=1}^{n}[b_i(E_i + E_{i-1})\tan\alpha_i + K_cW_ih_i + 2Q_i\sin\omega_ih_i]}{\sum_{i=1}^{n}[b_i(f_iE_i + F_{i-1}E_{i-1})]} \quad (8)$$

$$E_i = (\Psi_{i-1}E_{i-1}\Phi_{i-1} + F_sT_i - R_i)/\Phi_i \quad (9)$$

$$\Phi_{i-1} = (\sin\alpha_{i-1} - \lambda f_{i-1}\cos\alpha_i)\tan\phi_{i-1}' + (\cos\alpha_{i-1} + \lambda f_{i-1}\sin\alpha_{i-1})F_s \quad (10)$$

$$\Phi_i = (\sin\alpha_i - \lambda f_i\cos\alpha_i)\tan\phi_i' + (\cos\alpha_i + \lambda f_i\sin\alpha_i)F_s \quad (11)$$

$$R_i = [W_i \cos \alpha_i - K_c W_i \sin \alpha_i + Q_i \cos(\omega_i - \alpha_i) - U_i] \tan \phi_i' + c_i' b_i \sec \alpha_i \quad 12.$$

$$T_i = W_i \sin \alpha_i + K_c W_i \cos \alpha_i - Q_i \sin(\omega_i - \alpha_i) \quad 13.$$

In reality, R_i is sum of the components of all the forces acting on a slice contributing to the resisting force except the inter-slice normal forces, and T_i is sum of all the forces that contribute to the driving force that cause instability. As the F_s term exists on both sides of Equation 6, an iterative procedure has to be adopted to solve for F_s, with an assumed value in the first trial.

To incorporate the influence of stabilising piles in the safety analysis of slopes, a pile-stabilised slope as shown in Figure 4 with pile located at the k^{th} slice is considered. The slope is demarcated into three zones, namely, the pre-arching zone, the arching zone and the post-arching zone. The region k in Figure 4 represents the arching zone. The $(k - 1)^{th}$ and $(k + 1)^{th}$ slices are located to the right and left of the arching zone, respectively.

Figure 5 shows an enlarged view of the arching zone and the adjacent slices with the additional forces that occurs due to the introduction of piles. It should be noted that all the forces shown in Figure 3 also act on these slices, although they are omitted in Figure 5 to improve clarity. The width of the k^{th} slice is assumed to be the length of horizontal arching zone (Figure 1), given by:

$$l_a = \frac{D}{2}\sqrt{n^2 + 1} \quad 14.$$

From the analytical solutions presented in the previous section, the resultant pile force P_r is the difference between the force P_o acting on the right edge of arching zone and the force P_i acting on the left edge of the arching zone (Neeraj, 2019).

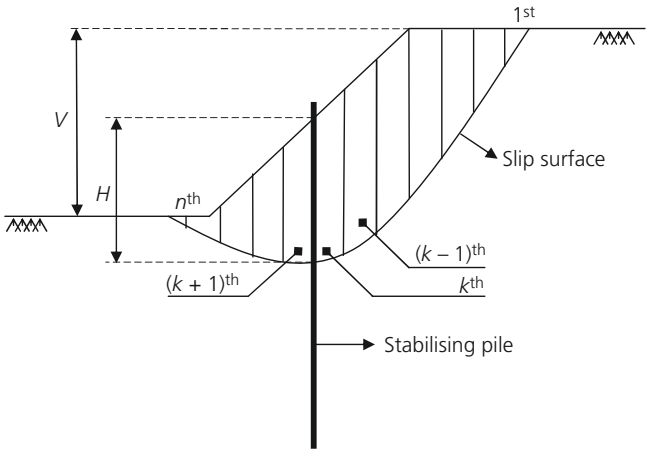

Figure 4. Pile-stabilised slope divided into slices

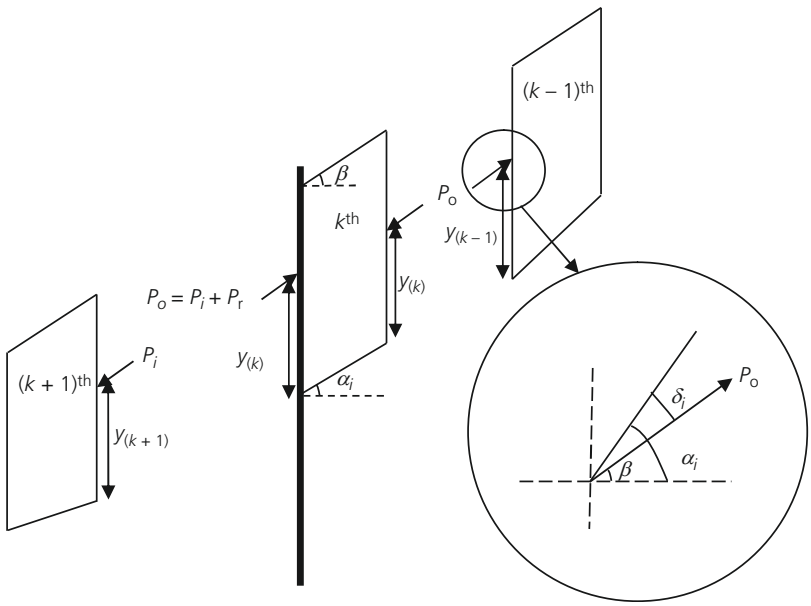

Figure 5. $(k + 1)^{th}$, k^{th} and $(k - 1)^{th}$ slices

$$P_{\mathrm{o}} = nDH\left[\left(\frac{\sqrt{n^2+1}}{n-1}\right)^{N-1}\left\{\frac{K_{\mathrm{an}}\gamma H\cos\beta}{1-C_1}\left(\frac{1}{1+C_1}-\frac{1}{2}\right)+\frac{C_2}{C_1}\left(\frac{1}{1+C_1}-1\right)+T\right\}+\frac{2\mathrm{c}\sqrt{\mathrm{N}}}{\mathrm{N}-1}\left\{\left(\frac{\sqrt{n^2+1}}{n-1}\right)^{N-1}-1\right\}\right] \quad (15)$$

$$P_{\mathrm{i}} = (n-1)DH\left[\frac{K_{\mathrm{an}}\gamma H\cos\beta}{1-C_1}\left(\frac{1}{1+C_1}-\frac{1}{2}\right)+\frac{C_2}{C_1}\left(\frac{1}{1+C_1}-1\right)+T\right] \quad (16)$$

The points of application of lateral thrusts P_{o} and P_{i} are given by $y_{k-1} = M_{\mathrm{o}}/P_{\mathrm{o}}$, and $y_{k+1} = M_{\mathrm{i}}/P_{\mathrm{i}}$, respectively, where M_{o} and M_{i} are corresponding moments along the slip surface. The detailed derivation of resultant forces (P_{o} and P_{i}) and moments (M_{o} and M_{i}) in the pre-arching and post-arching zones and the points of action (y_{k-1} and y_{k+1}) is presented in Appendix B.

The forces P_{o} and P_{i} are considered as external forces acting on the corresponding slices. They are resolved in the normal and tangential direction with respect to base of each slice and incorporated in R_{i} and T_{i} of corresponding slices as shown in Equations 17–20.

$$R_{k-1} = \left[W_{k-1}\cos\alpha_{k-1} - K_c W_{k-1}\sin\alpha_{k-1} + Q_{k-1}\cos(\omega_{k-1}-\alpha_{k-1}-1) - U_{k-1} + \frac{P_o}{s}\sin\delta\right]\tan\phi' + c_{k-1}b_{k-1}\sec\alpha_{k-1} \quad (17)$$

$$T_{k-1} = \left[W_{k-1}\sin\alpha_{k-1} + K_c W_{k-1}\cos\alpha_{k-1} + Q_{k-1}\sin(\omega_{k-1}-\alpha_{k-1}-1) - \frac{P_o}{s}\cos\delta\right] \quad (18)$$

$$R_{k+1} = \left[W_{k+1}\cos\alpha_{k+1} - K_c W_{k+1}\sin\alpha_{k+1} + Q_{k+1}\cos(\omega_{k+1}-\alpha_{k+1}-1) - U_{k+1} - \frac{P_i}{s-D}\sin\delta\right]\tan\phi' + c_{k+1}b_{k+1}\sec\alpha_{k+1} \quad (19)$$

$$T_{k+1} = \left[W_{k+1}\sin\alpha_{k+1} + K_c W_{k+1}\cos\alpha_{k+1} + Q_{k+1}\sin(\omega_{k+1}-\alpha_{k-1}-1) + \frac{P_i}{s-D}\cos\delta\right] \quad (20)$$

where, $\delta = |\alpha - \beta|$ is the inclination of resultant additional force (P_{o} or P_{i}) with reference to the respective slice base as shown in Figure 5. Since the k^{th} slice has equal forces acting from both sides ($P_{\mathrm{i}} + P_{\mathrm{r}} = P_{\mathrm{o}}$, on the right edge and P_{o} on the left edge), R_k and T_k remain unchanged. However, the moment equilibrium of the slice is influenced by these forces as their lines of action differ. Specifically, an additional moment M_{a} is generated as given in Equation 21.

$$M_{\mathrm{a}} = \left[y_{k+1}\left\{\frac{P_{\mathrm{i}}}{s-D}-\frac{P_{\mathrm{o}}}{s}\right\} + \frac{P_{\mathrm{o}}}{s}\left\{b_k\tan\alpha_k + \frac{b_{k-1}}{2}\tan\alpha_{k-1}\right\} + \frac{P_i b_{k+1}}{2(s-D)}\tan\alpha_{k+1}\right]\cos\beta \quad (21)$$

Since the present method does not consider the pile's contribution as an additional component explicitly, the equation for F_s (Equation 6) remains the same. However, the scale factor λ needs to be modified to incorporate the additional moment M_{a} (Equation 21) developed on k^{th} slice as follows,

$$\lambda_{\mathrm{m}} = \frac{\sum_{i=1}^{n}[b_i(E_i+E_{i-1})\tan\alpha_i + K_c W_i h_i + 2Q_i\sin\omega_i h_i] + M_{\mathrm{a}}}{\sum_{i=1}^{n}[b_i(f_i E_i + f_{i-1}E_{i-1})]} \quad (22)$$

The modified scale factor, λ_{m}, has to be used in Equations 7, 10 and 11 for F_s calculation.

Algorithm to obtain factor of safety

As indicated earlier, an iterative procedure is required to solve for the factor of safety. An iterative algorithm was developed for determining the critical slip surface and corresponding F_s for a given pile-stabilised slope. The steps involved in the iteration are as follows.

1. Input the slope geometry (height, V and slope angle, β); soil properties (γ, c and ϕ); and pile parameters (D and S).
2. Divide the whole slope into a number of slices.
3. Input pile location (k) and compute the length of the soil-arching zone (l_a).
4. Choose an arbitrary slip surface and input entry and exit points.
5. Calculate the resultant forces acting on k^{th}, $(k-1)^{th}$ and $(k+1)^{th}$ slices (P_r, P_o and P_i) and the additional moment (M_a) developed due to the introduction of the piles, using Equations 4, 15, 16, and 21, respectively.
6. Calculate R_i and T_i for all the slices using Equations 12 and 13, respectively.
7. Modify R_i and T_i for $(k-1)^{th}$ slice and $(k+1)^{th}$ slice using Equations 17–20.
8. Define the inter-slice function $f(x)$. A half-sine function is assumed here:

$$f(x) = \sin\left[\pi\left(\frac{x - x_{min}}{x_{max} - x_{min}}\right)\right]$$

where, x_{max} and x_{min} are abscissa of entry and exit points of the failure surface, respectively, and x denotes the abscissa of midpoint of each slice.

9. Assume an initial value for F_s and λ_m. The number of iterations required depends on the initial values assumed. However, the final values of F_s and λ_m do not vary with the assumed initial values. An effective transfer of inter-slice normal force requires the assumed F_s to satisfy Equation 7 (Zhu *et al.*, 2005). In general, for the first iteration, it can be assumed that $F_s = 1$ and $\lambda_m = 0$.
10. Calculate Ψ_i and Φ_i and for all slices using Equations 7 and 11.
11. Calculate F_s using Equation 6.
12. With F_s obtained from step 11 and the assumed value of λ_m, repeat steps 10 and 11 once more for the improved values of Φ_i, Ψ_i and F_s.
13. Calculate E_i using Equation 9.
14. Calculate λ_m using Equation 22.
15. With the updated values of F_s and λ_m, repeat steps 10–15 until the difference in the values of F_s and λ_m for two consecutive iterations fall below the tolerances t_1 and t_2, respectively. A tolerance of 0.001 was considered for both cases in this analysis.
16. Store the F_s value for the chosen slip surface.
17. Choose a different slip surface and return to step 4. Repeat up to step 17 for all the possible slip surfaces.
18. Find the minimum of all the F_s values obtained in step 17 to obtain the factor of safety and the critical slip surface of the pile-stabilised slope.

The above algorithm was coded in Matlab software (R2020b). The algorithm can also be used to obtain the F_s of soil slopes that are not stabilised by piles if R_i and T_i are calculated using Equations 12 and 13, respectively, for all slices and the scale factor (λ) is determined using Equation 8. Also, for the no-pile condition, the division of the slope into three zones is not needed. Figure 6 shows the typical output plot with various slip surfaces considered and the failure surface corresponding to the minimum F_s, for a particular pile position and slope angle. The abscissa and ordinate represent the respective horizontal and vertical dimensions of the model considered in the analysis. The critical slip surface is represented by red colour and the green lines represent the ground surface. The line with star marks at either ends denotes the location of the pile.

Comparison of algorithm with finite-element modelling and the limit equilibrium method

Factor of safety values for soil slopes with and without piles obtained from the proposed algorithm were compared with that determined using finite element modelling. Slopes without pile were modelled both in Plaxis 3D software and the Slope/W program of the GeoStudio software package. The Slope/W program is widely used to obtain the factor of safety of normal soil slopes. Pile-stabilised slopes were simulated only in Plaxis 3D as Slope/W program is a two-dimensional modelling tool.

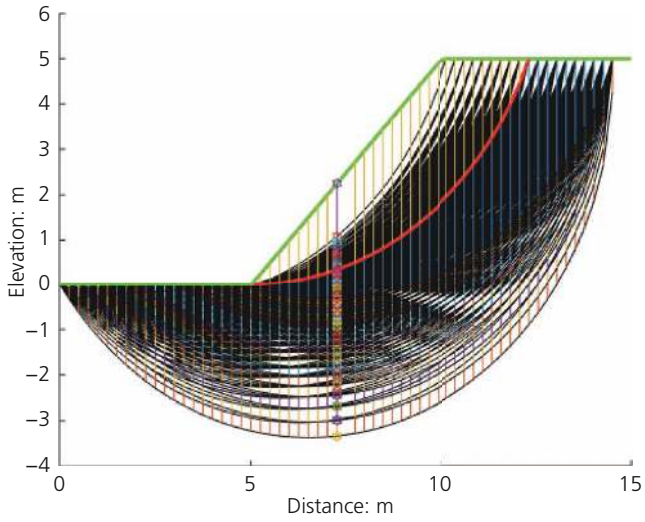

Figure 6. Typical output plot with different slip surfaces and failure surface generated in Matlab

Table 1. Material properties adopted in numerical modelling

	Soil A	Soil B	Pile
γ: kN/m^3	20	20	25
E: kPa	5×10^3	3.5×10^3	7×10^7
μ	0.25	0.25	0.15
c: kPa	0	40	–
ϕ: °	32	20	–
ψ: °	0	0	–

A soil slope having a height of 5 m and slope angle (β) of 26.6° (1V:2H) was modelled using various soil conditions and pile parameters as shown in Table 1. Two different soil conditions represented as Soil A (sand) and Soil B (c–ϕ soil) were chosen for the analyses. In the case of the pile-stabilised slope, a row of 0.3 m and 1 m dia. piles at a spacing of three times the diameter was considered. Modelling of slope sections with different number of piles was carried out and the results were essentially the same. The model presented here was the one with nine piles.

Figure 7 displays the slope model constructed in limit equilibrium slope stability mode of Slope/W. Morgenstern–Price analysis type was selected with a half-sine side function as adopted in the proposed algorithm. The soil was characterised as Mohr–Coulomb material and the phreatic line was assumed to be at a greater depth below base of the model. The potential slip surfaces for analysis were defined using entry and exit points with the specified 'radius tangential lines' intrinsic option available in the program.

In case of Plaxis 3D analysis, three-dimensional (3D) models of soil slope (and piles) were generated using 10-nodded tetrahedral elements. The built-in 'soil and interface' material type was selected to model soil and piles. The soil was modelled as Mohr–Coulomb material. The piles were modelled as concrete piles using the linear-elastic material model. The boundary condition at all the vertical surfaces was set to normally fixed. The horizontal surface at the base was fully restrained. The slope surface and the horizontal surfaces at the top were set to free. Sufficient depth of soil was provided below the pile tip so that the influence of boundary was negligible. The effect of construction sequence and pile installation were not considered in the present analysis. The soil mass and the piles were activated in the initial phase and a K_o calculation type was chosen. A null plastic analysis in phase 2 of the staged construction loading type was carried out to activate the gravity loads due to the soil mass and the row of piles. The plastic analysis was followed by the inbuilt safety analysis with updated mesh to determine the factor of safety of pile-stabilised slopes. The principle of strength reduction was used to obtain the factor of safety. Factor of safety is defined as the ratio of maximum available shear strength to minimum shear strength required for equilibrium. The standard Coulomb condition is introduced to strength reduction method to obtain Equation 23 for factor of safety (Brinkgreve *et al*., 2018).

$$\text{23.}\quad \text{Factor of safety} = \frac{c - \sigma_m \tan\phi}{c_r - \sigma_m \tan\phi_r}$$

where, c and ϕ are input strength parameters which are reduced to c_r and ϕ_r, the minimum required strength parameters, and σ_n is the normal stress component. In the strength reduction approach of Plaxis 3D, both c and ϕ are reduced by a common multiplier ΣM_{sf} as given in Equation 24. This parameter is incrementally increased till failure and the value of M_{sf} at failure is reported as factor of safety (Brinkgreve *et al*., 2018).

$$\text{24.}\quad \sum M_{sf} = \frac{c}{c_r} = \frac{\tan\phi}{\tan\phi_r}$$

Figure 8 shows the total deformation contour obtained from the safety analysis of pile-stabilised slope in Plaxis 3D. Table 2 summarises the F_s values for slopes without piles for different soil types obtained from the proposed algorithm and finite-element modelling.

The comparison of F_s values of pile-stabilised slopes for the case of 0.3 and 1 m dia. piles, estimated using Plaxis 3D, and the developed

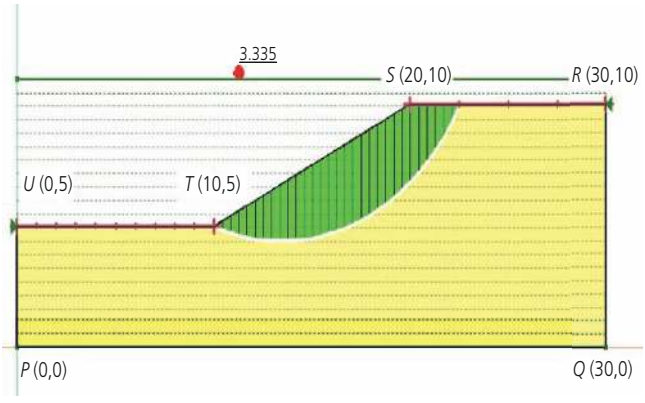

Figure 7. F_S computation results in slope/W, GeoStudio

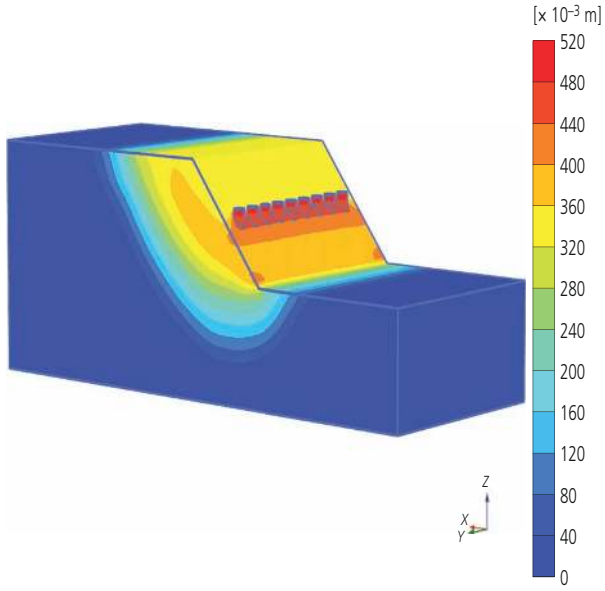

Figure 8. Total deformation contour after safety analysis of pile-stabilised slope model in Plaxis 3D

Table 2. Comparison of F_s values obtained from numerical modeling and proposed algorithm for slopes without piles

Method	Soil A	Soil B
GeoStudio (slope/W)	1.55	3.15
Plaxis 3D	1.53	3.08
Proposed algorithm	1.52	3.15

Table 3. Comparison of F_s values obtained from numerical modeling and proposed algorithm for pile-stabilised slopes

Pile diameter	Method	Soil A	Soil B
0.3 m	Plaxis 3D	1.72	3.32
0.3 m	Proposed algorithm	1.71	3.42
0.3 m	'Additional term' method	1.94	3.83
1.0 m	Plaxis 3D	2.15	3.92
1.0 m	Proposed algorithm	1.98	4.03
1.0 m	'Additional term' method	2.47	4.31

algorithm are presented in Table 3. The F_s values for the same slope and pile-dimensions, when computed by taking the pile contribution explicitly as an additional term, are also presented in Table 3. This was obtained by adding P (Equation 1) to the numerator of equation for F_s (Equation 6) wherein R_i, t_i and λ were obtained using Equations 12, 13 and 8, respectively, as discussed previously for the case of non-stabilised slopes.

As is evident from the tables, the factor of safety values for both normal and stabilised slopes predicted using the proposed method were in close agreement with that obtained from the numerical analyses. This implies that the proposed algorithm can be used to compute the F_s quickly, unlike the finite-element packages which require a significant amount of time to generate a model and calculate the results. It can be observed from Table 3 that considering the resistance offered by piles as an additional term in the equation for F_s, as conventionally done in practice, leads to an over-prediction. The 'additional term' method also fails to capture the effect of pile location. In reality, the F_s varies with the location of piles, as discussed in next section.

Change in critical failure plane

The installation of piles in a slope modifies its critical slip surface. The existing practices do not consider the change in critical slip surface and compute the factor of safety corresponding to the same slip surface as that of un-stabilised slopes. The proposed algorithm identifies the new critical slip surface formed due to the introduction of piles and computes the F_s corresponding to the new surface. To demonstrate the modification of slip surface due to the introduction of stabilising piles, the analyses were carried out for without and with stabilising piles cases using the proposed algorithm. Piles having a diameter of 1 m spaced at a centre-to-centre distance, n = 3, in a typical c–ϕ soil slope with c = 30 kN/m^2, ϕ = 20°, unit weight, γ = 20 kN/m^3, and slope angle β = 26.5 (2H:1V) were considered for the analyses. When all other factors are kept constant, the variation in the critical slip surfaces for the case of without and with stabilising piles obtained using the proposed algorithm is given in Figures 9(a) and 9(b), respectively. The colour codes adopted for Figure 6 are applicable to Figure 9 as well.

Determination of pile location and spacing

The factor of safety of pile-stabilised slopes is influenced by the location of the pile. Currently, the determination of optimal location of pile (OPL) is a time-consuming task which involves multiple finite-element modelling iterations, consuming considerable amounts of time. A new a straightforward technique to determine the OPL is presented in this work. The distance of the pile from the toe of the slope can be easily taken as an additional variable in the proposed

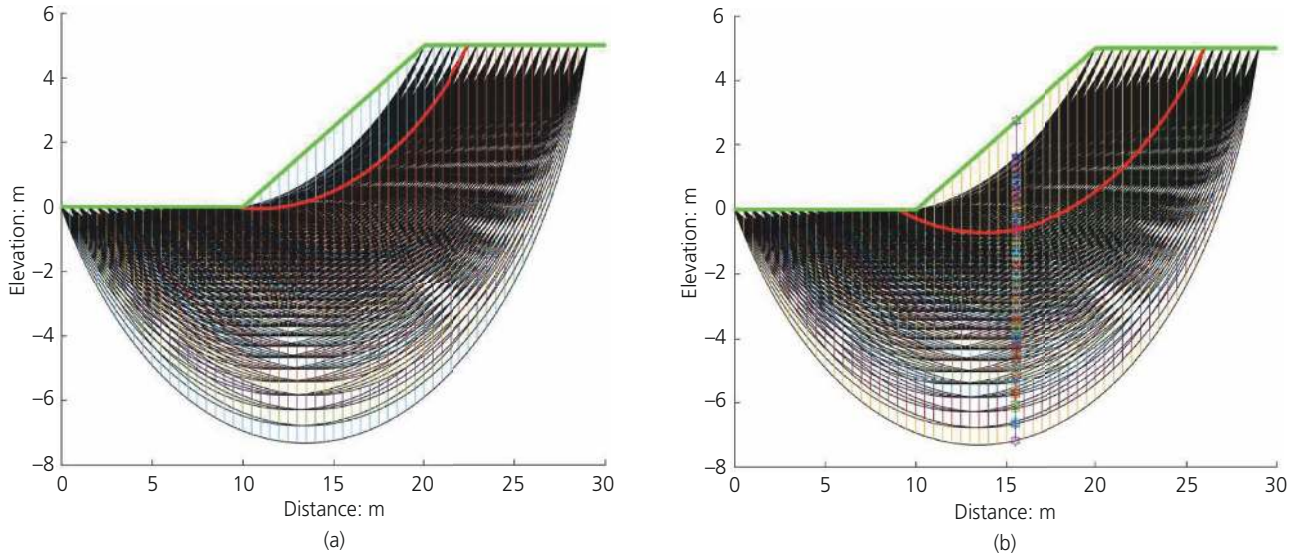

Figure 9. Critical slip surface generated using proposed algorithm (a) without pile and (b) with pile

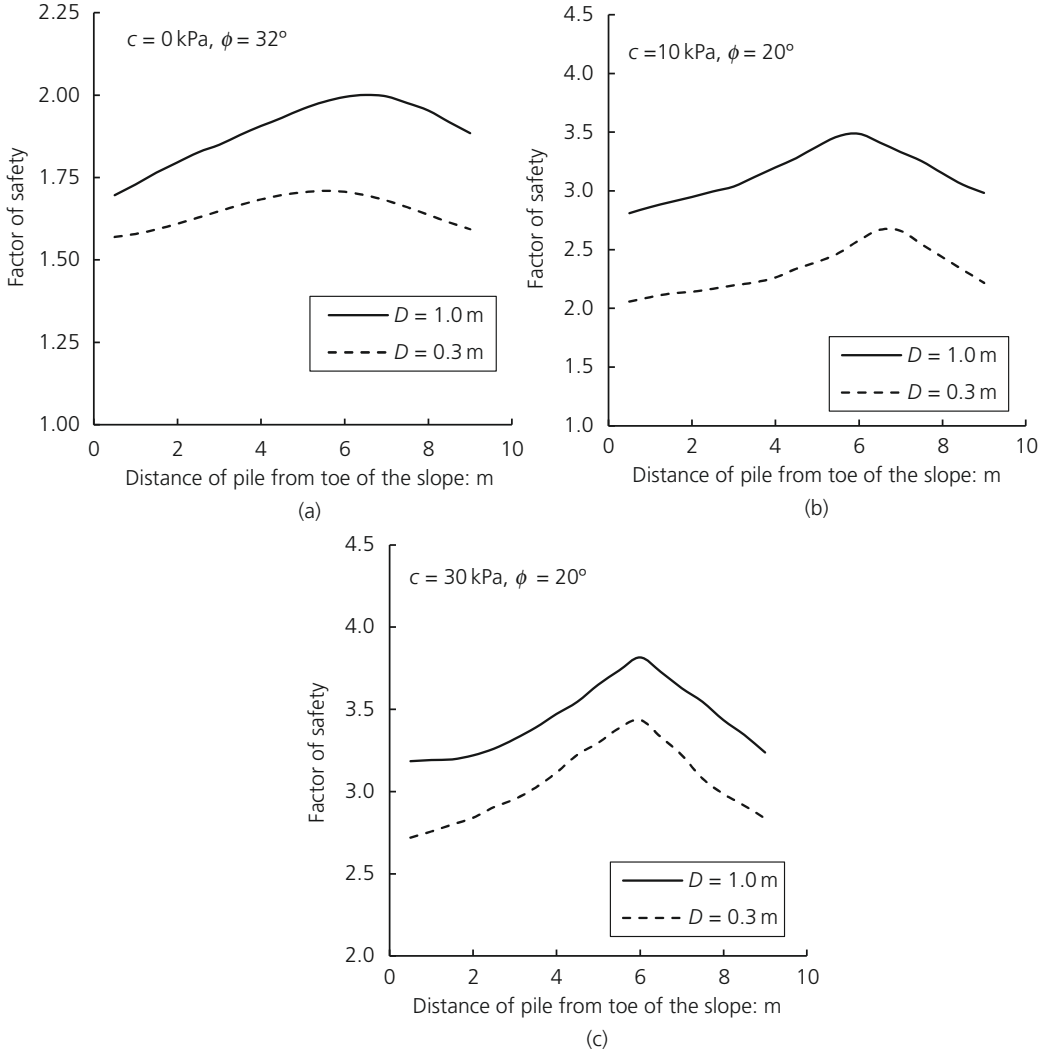

Figure 10. Variation of F_s with location of the piles: (a) soil (i), (b) soil (ii) and (c) soil (iii)

algorithm presented in the previous section and the F_s value corresponding to each pile location can be computed. Three typical scenarios, (i) $c = 0\ \text{kN/m}^2$, $\phi = 32°$, (ii) $c = 10\ \text{kN/m}^2$, $\phi = 20°$ and (iii) $c = 30\ \text{kN/m}^2$, $\phi = 20°$, were considered. A pile-stabilised slope installed with (*i*) $D = 0.3$ m and (*ii*) $D = 1$ m piles, spaced at a center-to-center distance, $n = 3$, and a slope angle $\beta = 26.5°$ (2H:1V) was adopted. The unit weight of soil was assumed as $20\ \text{kN/m}^3$. The total length of the base of the slope was adopted as 10 m. The variation of F_s with the location of pile for cases (i)–(iii) is presented in Figure 10(a)–(c).

The optimal location of pile obtained using the proposed method is in accordance with the results of past finite-element analyses found in literature. Hassiotis *et al*. (1997) suggested that the piles installed between the middle and the crest of the slope are most effective. In case of homogenous purely cohesive soil, Lee *et al*. (1995) showed that the most effective position of piles is close to the crest of the slope. The finite-element analysis presented in the paper by Cai and Ugai (2000) indicates that the piles located at the middle of the slope provide the highest factor of safety. Ausilio *et al*. (2001) also suggest placing the piles in the upper-middle portion of the slope for efficient stabilisation. As can be observed from Figure 10, the F_s values initially increase with the distance of pile from the toe of the slopes, reach a peak value and then decrease as the piles move further away from the toe. In case of sandy soil, the maximum factor of safety is obtained when the piles are located around the mid-slope. On the other hand, as the soil becomes cohesive, the maximum F_s value is found to occur at a pile location above the mid-slope. However, the location of pile corresponding to the peak value of F_s can not be readily called the OPL as it is also influenced by various other factors, for example, the access to the slope, space for construction and so on. Nevertheless, the proposed algorithm can be easily used to obtain the variation of factor of safety with location of pile, which in turn can be used by engineers to choose the location based on other field constraints.

The variation of F_s with the ratio of pile-spacing to diameter ($n = s/D$; $D = 0.3$) is presented in Figure 11 for the case of soils (i)–(iii). As the soil-arching effect is more significant when the piles are placed closer, the resistance they offer will be greater. Therefore, higher F_s is found to occur at smaller pile-spacing. Further, it can be observed that, beyond the pile-spacing of 4–5D, the change in F_s is negligible, because of lower pile-contribution.

Conclusions

In this work, a new algorithm is proposed to compute the factor of safety of pile-stabilised slopes. The proposed algorithm involves an iterative procedure which models the progressive transfer of additional resistance offered by piles. The pile-stabilised slope is divided into three zones (pre-arching, arching and post-arching zone) and a pressure-based method proposed by Neeraj and Thiyyakkandi (2020) is extended to obtain the force on each zone. Thereby, the effect of soil arching on the load-transfer mechanism of pile-stabilised slopes was intrinsically incorporated in the proposed algorithm. The comparison between F_s values computed using the proposed algorithm and those obtained using finite-element modelling showed that the algorithm can be used as a quick, simple and reliable technique to estimate the factor of safety of pile-stabilised slopes. The conventional method of computing F_s wherein the pile-contribution is considered as an additional term, was found to over-predict the values. Unlike the conventional methods, the proposed algorithm incorporates the modified slip surface while computing the F_s, which significantly affects the estimated value. Subsequently, the variation of F_s with the pile location along the slope was studied. It was found that, for frictional soil, the mid-slope was the ideal location of the pile, while, as the cohesion value increased, the maximum F_s occurred when the piles were placed above the middle of slope. The factor of safety was found to reduce with an increase in pile-spacing due to poor contribution from the pile. Apparently, a pile-spacing greater than four to five times the diameter of piles was found to be ineffective in stabilising the pile. However, the optimal pile location and spacing should only be determined by studying other field constraints and the cost involved. The experimental validation of the proposed method is also warranted before field use.

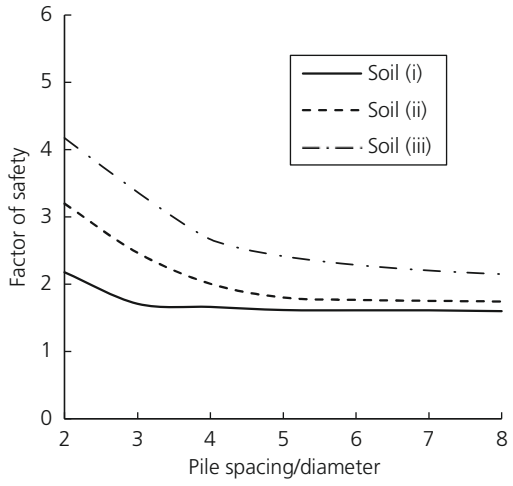

Figure 11. Variation of F_s with pile spacing

Acknowledgments

The first author gratefully acknowledges the financial support provided by the Ministry of Education (MoE), India, for completion of this work.

Appendix

A: formulation of vertical average stress $\overline{\sigma}_v$

The enlarged view of the differential element $EFF'E'$ (Figure 2) is shown in Figure 12. The triangle LFF' is in equilibrium state, and therefore, it can be ignored in the analysis of vertical equilibrium of the whole differential element (He *et al*., 2015a; Neeraj and Thiyyakkandi, 2020). The minor principal stress σ_3 acts on plane LF', which can be resolved in vertical direction to obtain σ_{3v} as

$$\sigma_{3v} = \sigma_3 \frac{\sin\xi\cos\beta}{\cos(\xi+\beta)} \quad (25)$$

Using the principles of origin of planes, it can be proved that:

$\xi = \frac{\pi}{4} + \frac{\phi}{2} - \theta_1$; $\theta = \frac{1}{2}\left(\phi - \beta + \cos^{-1}\frac{\sin\beta}{\sin\phi}\right)$; and
$\theta_1 = \frac{1}{2}\left(\phi + \beta + \cos^{-1}\frac{\sin\beta}{\sin\phi}\right)$

where θ is the angle between the slip plane and the slope surface; θ_1 is the angle between the slip plane and the horizontal; β is the slope angle; and ϕ is the angle of internal friction. Shear stress at face EE' is given by:

$$\tau = c + \sigma_h \tan\phi = c + (k_{an}\overline{\sigma}_v + T)\tan\phi \quad (26)$$

Considering the vertical force equilibrium of the differential element dz,

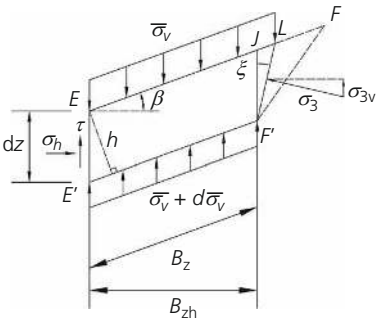

Figure 12. Enlarged view of the differential element in the vertical arching zone

$$\tau dz + (\overline{\sigma}_{\mathrm{v}} + d\overline{\sigma}_{\mathrm{v}})B' + \sigma_{3\mathrm{v}}dz - \overline{\sigma}_{\mathrm{v}}B' - \sigma_h \tan\beta dz - \gamma B' h = 0 \quad (27)$$

Where $B' = (H - z)\cos\theta_1/\sin\theta$ and $h = dz\cos\beta$.

Substituting Equation 26, Equation 2, Equation 25 and Equation 27 and rearranging,

$$\frac{d\overline{\sigma}_{\mathrm{v}}}{dz} + \overline{\sigma}_{\mathrm{v}}\left(\frac{C_1}{H-z}\right) + \frac{C_2}{H-z} - \gamma\cos\beta = 0 \quad (28)$$

C_1 and C_2 can be obtained from Equation 3.

Equation 22 is in the $dy/dx + Py = Q$ form and can be integrated using the method of integration factor to obtain $\overline{\sigma}_{\mathrm{v}}$.

$$\left[\overline{\sigma}_{\mathrm{v}} + \frac{\gamma\cos\beta(H-z)}{1-C_1} + \frac{\mathrm{C}_2}{\mathrm{C}_1}\right](H-z)^{-\mathrm{C}_1} = C \quad (29)$$

where, C is the constant of integration. Applying the boundary condition, $\overline{\sigma}_{\mathrm{v}} = 0$ at $z = 0$, in Equation 29 gives:

$$C = \left[\frac{\gamma\cos\beta H}{1-C_1} + \frac{C_2}{C_1}\right](H)^{-C_1} \quad (30)$$

Substituting for C (Equation 30) in Equation 29 and re-arranging,

$$\overline{\sigma}_{\mathrm{v}} = \frac{\gamma\cos\beta H}{1-C_1}\left[\left(1-\frac{z}{H}\right)^{C_1} - \left(1-\frac{z}{H}\right)\right] + \frac{C_2}{C_1}\left[\left(1-\frac{z}{H}\right)^{C_1} - 1\right] \quad (31)$$

B: resultant forces and point of action

The resultant reaction on pre-arching zone, P_{o}, and the resultant lateral force transferred to the post-arching zone, P_i, can be obtained by integrating the force per unit length along the depth.

$$P_{\mathrm{o}} = \int_0^H \sigma_{\mathrm{o}}(s)dz \quad \text{and} \quad P_{\mathrm{i}} = \int_0^H \sigma_{\mathrm{i}}(s-D)dz \quad (32)$$

Here, σ_o and σ_i are the stresses along the outer and inner planes of the arching zone, respectively (Figure 1). The stress σ_i is given by Equation 2 and the stress σ_o is related to σ_i as (Neeraj and Thiyyakkandi, 2020):

$$\sigma_{\mathrm{o}} = \sigma_{\mathrm{i}}\left(\frac{\sqrt{n^2+1}}{n-1}\right)^{N-1} + \frac{2c\sqrt{N}}{N-1}\left[\left(\frac{\sqrt{n^2+1}}{n-1}\right)^{N-1} - 1\right] \quad (33)$$

Substituting Equations 2 and 33 in Equation 32 and integrating yields,

$$P_{\mathrm{o}} = nDH\left[\left(\frac{\sqrt{n^2+1}}{n-1}\right)^{N-1}\left\{\frac{K_{\mathrm{an}}\gamma H\cos\beta}{1-C_1}\left(\frac{1}{1+C_1} - \frac{1}{2}\right) + \frac{C_2}{C_1}\left(\frac{1}{1+C_1} - 1\right) + T\right\} + \frac{2c\sqrt{N}}{N-1}\left\{\left(\frac{\sqrt{\mathrm{n}^2+1}}{\mathrm{n}-1}\right)^{N-1} - 1\right\}\right] \quad (34)$$

$$P_{\mathrm{i}} = (n-1)DH\left[\frac{K_{\mathrm{an}}\gamma H\cos\beta}{1-C_1}\left(\frac{1}{1+C_1} - \frac{1}{2}\right) + \frac{C_2}{C_1}\left(\frac{1}{1+C_1} - 1\right) + T\right] \quad (35)$$

To obtain the points of application of these forces, the moment about the point where the piles intersect the slip surface is taken, that is,

$$M_{\mathrm{o}} = \int_0^H \sigma_{\mathrm{o}}(s)(H-z)dz \quad \text{and} \quad M_{\mathrm{i}} = \int_0^H \sigma_{\mathrm{i}}(s-D)(H-z)dz \quad (36)$$

Using Equations 2, 33–36, the point of application of forces from the slip surface can obtained as:

$$h_{\mathrm{o}} = \frac{M_{\mathrm{o}}}{P_{\mathrm{o}}} \quad \text{and} \quad h_{\mathrm{i}} = \frac{M_{\mathrm{i}}}{P_{\mathrm{i}}} \quad (37)$$

REFERENCES

Ahmed S (2017) *Matlab Script for Slope Stability Calculations with Comsol Multiphysics*. PhD thesis, École de technologie supérieure, Université du Québec, Montreal, Canada.

Ashour M and Ardalan H (2012) Analysis of pile stabilized slopes based on soil-pile interaction. *Computers and Geotechnics* **39**: 85–97, https://doi.org/10.1016/j.compgeo.2011.09.001.

Atarigaya BD (2016) *Numerical Modeling and Simulation of the Stability of Earth Slopes*. PhD thesis, University of Ghana, Accra, Ghana.

Ausilio E, Conte E and Dente G (2001) Stability analysis of slopes reinforced with piles. *Computers and Geotechnics* **28(8)**: 591–611, https://doi.org/10.1016/S0266-352X(01)00013-1.

Brinkgreve R, Engin E and Swolfs W (2018) *PLAXIS 3D Tutorial Manual 2018*. Plaxis bv, Delft, the Netherlands.

Cai F and Ugai K (2000) Numerical analysis of the stability of a slope reinforced with piles. *Soils and Foundations* **40(1)**: 73–84, https://doi.org/10.3208/sandf.40.73.

Di Laora R, Maiorano RMS and Aversa S (2017) Ultimate lateral load of slope-stabilising piles. *Géotechnique Letters* **7(3)**: 237–244, https://doi.org/10.1680/jgele.17.00038.

Duncan JM (1996) State of the art: limit equilibrium and finite-element analysis of slopes. *Journal of Geotechnical Engineering* **122(7)**: 577–596, https://doi.org/10.1061/(ASCE)0733-9410(1996)122:7(577).

Ellis E, Durrani IK and Reddish DJ (2010) Numerical modelling of discrete pile rows for slope stability and generic guidance for design. *Géotechnique* **60(3)**: 185–195, https://doi.org/10.1680/geot.7.00090.

Firat S (2009) Stability analysis of pile-slope system. *Scientific Research and Essays* **4(9)**: 842–852, https://doi.org/10.5897/SRE.9000860.

Griffiths D and Lane P (1999) Slope stability analysis by finite elements. *Géotechnique* **49(3)**: 387–403, https://doi.org/10.1680/geot.1999.49.3.387.

Harrop-Williams K (1989) Arch in soil arching. *Journal of Geotechnical Engineering* **115(3)**: 415–419, https://doi.org/10.1061/(ASCE)0733-9410(1989)115:3(415).

Hassiotis S, Chameau J and Gunaratne M (1997) Design method for stabilization of slopes with piles. *Journal of Geotechnical and Geoenvironmental Engineering* **123(4)**: 314–323, https://doi.org/10.1061/(ASCE)1090-0241(1997)123:4(314).

He Y, Hemanta H, Noriyuki Y and Zheng H (2015a) Evaluating the effect of slope angle on the distribution of the soil-pile pressure acting on stabilizing piles in sandy slopes. *Computers and Geotechnics* **69**: 153–165, http://dx.doi.org/10.1016/j.compgeo.2015.05.006.

He Y, Hemanta H, Noriyuki Y *et al.* (2015b) Estimation of lateral force acting on piles to stabilize landslides. *Natural Hazards* **79(3)**: 1981–2003, https://doi.org/10.1007/s11069-015-1942-0.

Ito T and Matsui T (1975) Methods to estimate lateral force acting on stabilizing piles. *Soils and Foundations* **15(4)**: 43–59, https://doi.org/10.3208/sandf1972.15.443.

Jeong S, Kim B, Won J and Lee J (2003) Uncoupled analysis of stabilizing piles in weathered slopes. *Computers and Geotechnics* **30(8)**: 671–682, https://doi.org/10.1016/j.compgeo.2003.07.002.

Kourkoulis R, Gelagoti F, Anastasopoulos I and Gazetas G (2011) Hybrid method for analysis and design of slope stabilizing piles. *Journal of Geotechnical and Geoenvironmental Engineering* **138(1)**: 1–14, https://doi.org/10.1061/(ASCE)GT.1943-5606.0000546.

Lee C, Hull T and Poulos H (1995) Simplified pile-slope stability analysis. *Computers and Geotechnics* **17(1)**: 1–16, https://doi.org/10.1016/0266-352X(95)91300-S.

Li X and Wei S (2018) A calculation method for the distribution of lateral force acting on stabilizing piles considering soil arching effect. *Indian Geotechnical Journal* **49(1)**: 132–139, https://doi.org/10.1007/s40098-018-0307-5.

Liang R and Zeng S (2002) Numerical study of soil arching mechanism in drilled shafts for slope stabilization. *Soils and Foundations* **42(2)**: 83–92, https://doi.org/10.3208/sandf.42.283.

Liang RY, Joorabchi AE and Li L (2014) Analysis and design method for slope stabilization using a row of drilled shafts. *Journal of Geotechnical and Geoenvironmental Engineering* **140(5)**: 04014001, https://doi.org/10.1061/(ASCE)GT.1943-5606.0001070.

Lirer S (2012) Landslide stabilizing piles: experimental evidences and numerical interpretation. *Engineering Geology* **149–150**: 70–77, https://doi.org/10.1016/j.enggeo.2012.08.002.

Morgenstern N and Price V (1965) The analysis of the stability of general slip surfaces. *Géotechnique* **15(1)**: 79–93, https://doi.org/10.1680/geot.1965.15.1.79.

Neeraj CR (2019) *Analysis of Pile-Stabilised Slopes Incorporating Horizontal and Vertical Arching*. MS thesis, Indian Institute of Technology, Palakkad, India.

Neeraj CR and Thiyyakkandi S (2020) Estimation of lateral pile resistance incorporating soil arching in pile-stabilized slopes. *Geomechanics and Engineering* **23(5)**: 481–491, https://doi.org/10.12989/gae.2020.23.5.481.

Summersgill FC, Kontoe S and Potts DM (2018) Stabilisation of excavated slopes in strain-softening materials with piles. *Géotechnique* **68(7)**: 626–639, https://doi.org/10.1680/jgeot.17.P.096.

Song Y-S, Hong W-P and Woo K-S (2012) Behavior and analysis of stabilizing piles installed in a cut slope during heavy rainfall. *Engineering Geology* **129-130**: 56–67, https://doi.org/10.1016/j.enggeo.2012.01.012.

Tsuchida T and Athapaththu A (2014) Practical slip circle method of slices for calculation of bearing capacity factors. *Soils and Foundations* **54(6)**: 1127–1144, https://doi.org/10.1016/j.sandf.2014.11.008.

Won J, You K, Jeong S and Kim S (2005) Coupled effects in stability analysis of pile-slope systems. *Computers and Geotechnics* **32(4)**: 304–315, https://doi.org/10.1016/j.compgeo.2005.02.006.

Zhu D, Lee C, Qian Q and Chen G (2005) A concise algorithm for computing the factor of safety using the Morgenstern-Price method. *Canadian Geotechnical Journal* **42(1)**: 272–278, https://doi.org/10.1139/t04-072.

How can you contribute?

To discuss this paper, please submit up to 500 words to the editor at journals@ice.org.uk. Your contribution will be forwarded to the author(s) for a reply and, if considered appropriate by the editorial board, it will be published as a discussion in a future issue of the journal.